Heat capacity and Joule-Thomson coefficient of selected n-alkanes at 0.1 and 10 MPa in broad temperature ranges

Regueira Muñiz, Teresa; Varzandeh, Farhad; Stenby, Erling Halfdan; Yan, Wei

Published in:
Journal of Chemical Thermodynamics

Link to article, DOI:
10.1016/j.jct.2017.03.034

Publication date:
2017

Document Version
Peer reviewed version

Heat capacity and Joule-Thomson coefficient of selected n-alkanes at 0.1 and 10 MPa in broad temperature ranges

Teresa Regueira, Farhad Varzandeh, Erling H. Stenby, Wei Yan*

Center for Energy Resources Engineering (CERE), Department of Chemistry, Technical University of Denmark, DK-2800 Kgs. Lyngby, Denmark

*Corresponding author: E-mail: weya@kemi.dtu.dk; Tel.:+45 45252379

Abstract

Isobaric heat capacity of six n-alkanes, i.e. n-hexane, n-octane, n-decane, n-dodecane, n-tetradecane and n-hexadecane, was determined with a Calvet type differential heat-flux calorimeter at 0.1 and 10 MPa in a broad temperature range. The measured isobaric heat capacity data were combined with the literature density data for these n-alkanes to determine the corresponding Joule-Thomson coefficients. Four different EoSs, Soave-Redlich-Kwong, Peng-Robinson, Perturbed Chain Statistical Associating Fluid Theory, and Soave-Benedict-Webb-Rubin, were used to model the heat capacities and Joule-Thomson coefficients. Moreover, the Joule-Thomson inversion curves for these n-alkanes were also calculated by the four EoSs.

Keywords: n-alkane, heat capacity, Joule-Thomson coefficient, high pressure, high temperature

1. Introduction

Accurate knowledge of heat capacity as a function of temperature and pressure is important to many industrial applications because this property is needed in energy balances, in entropy and enthalpy calculations or in the study of phase transitions. Heat capacity also provides information on the molecular structure, such as indicating structural changes [1-3]. As one of the second order derivative properties of Gibbs energy, heat capacity is difficult to describe accurately and modelling of this property is a demanding test for equations of state [2-5].

Normal alkanes are constituents of the reservoir fluids, and their heat capacity values are of importance for the oil and gas industry in order to develop and validate models which could be further applied to the real reservoir fluids in broad temperature and pressure ranges. In the present work we report measurements of specific isobaric heat capacity (C_p) for six n-alkanes, i.e. n-hexane, n-octane, n-decane, n-dodecane, n-tetradecane and n-hexadecane at two different pressures of 0.1 and 10 MPa up to 483.15 K or a lower temperature if phase transition occurs or endothermic convection is observed during the measurement. Zábranský and co-workers [6-9] have given four comprehensive reviews on isobaric and saturation heat capacity data, containing around 2000 organic and inorganic liquids with melting points below 573 K since 1991. The reviews include the C_p correlations with temperature at ambient pressure. Taking into account the recommended values of C_p for the n-alkanes reported in the most recent review by Zábranský et al. [9], one can see that there is scarcity of data at temperatures higher than 373.15 K at ambient or saturation pressure. For instance, among these recommended C_p values [9] there are only two data series with C_p values at temperatures higher that 373.15 K for n-decane, which were reported by Grigor'ev et al. [10] and Kuznetsov et al. [11]; for n-dodecane [12], n-tetradecane [13] and n-hexadecane [14] there is only one data series with temperatures higher than 373.15 K for each of them [12-14]. Moreover, data on C_p of these n-alkanes at high

pressures is far from comprehensive. To the best of our knowledge, C_p data for n-hexane at high pressures was measured by Bessières et al. [15] up to 100 MPa and temperatures up to 373.15 K, by González-Salgado et al. [1] up to 60 MPa and 323.15 K and by Zaripov et al. up to 147 MPa and 348.17 K. For n-octane, Banipal et al. [16] published C_p values up to 10 MPa and 373.15 K. Regarding n-decane, Banipal et al. [16] reported C_p values up to 10 MPa and 373.15 K, Bessières et al. [17] up to 10 MPa and 372.27 K and González-Salgado et al. [1] up to 60 MPa and 323.15 K. As for n-dodecane, Bessières et al. [4] measured values up to 100 MPa and 373.15 K and González-Salgado et al. [1] up to 60 MPa and 323.15 K, also Khasanshin et al. [18] reported values of this property up to 140 MPa and 433.15 K obtained from heat capacity and density data at atmospheric pressure, as well as speed of sound data as a function of temperature and pressure. As regards n-tetradecane, high pressure data was previously published by González-Salgado et al. [1] up to 60 MPa and 323.15 K and calculated from speed of sound data by Khasanshin et al. [19] up to 140 MPa and 433.15 K. Finally, for n-hexadecane, C_p data at high pressures were previously reported by Banipal et al. [16] up to 10 MPa and 373.15 K. These existing data show that an effort has been made to report accurate values of C_p of n-alkanes in broad temperature and pressure ranges, however it is also shown that there is still lack of accurate C_p data at high temperature and pressure conditions.

The Joule-Thomson coefficient (μ_{JT}) indicates the rate of temperature change with pressure during an isenthalpic expansion. Knowledge of this coefficient is important for many disciplines including reservoir engineering. Isentropic expansion of fluid usually causes cooling and this may lead to wax formation in the well if the oil is around its cloud point near the wellbore and the Joule-Thomson coefficient is positive [20]. Joule-Thomson coefficients can also be negative, corresponding to the so-called reverse Joule-Thomson effect, i.e., temperature increase after depressurization, which can damage the surface production facilities and affect well integrity and safety [21,22]. Accurate description of the Joule-Thomson coefficient allows better understanding of the reservoir fluid behavior and prediction of the unexpected behavior such as heating upon expansion. For high pressure-high temperature reservoirs, μ_{JT} is fundamental in the design and material selection, operation and maintenance of production operations [21,23,24]. This coefficient is also needed as an input in the interpretation of temperature log data and prediction of the temperature profiles in the wells [25,26]. The Joule-Thomson coefficients for n-hexane, n-octane, n-decane, n-dodecane, n-tetradecane and n-hexadecane are determined in the present work indirectly by utilizing both C_p and density data at the considered temperature and pressure conditions. Furthermore calculations of this coefficient as well as of C_p for the aforementioned n-alkanes through Soave-Redlich-Kwong (SRK) [27], Peng-Robinson (PR) [28], Perturbed Chain Statistical Associating Fluid Theory (PC-SAFT) [29], and Soave-Benedict-Webb-Rubin (Soave-BWR) [30] EoSs are presented in this work in order to evaluate the performance of the models.

In a pT diagram the locus where the Joule-Thomson coefficient is zero constitutes the inversion curve. The curve defines the border between heating (the Joule-Thomson coefficient smaller than zero) and cooling (the coefficient larger than zero) in Joule-Thomson processes. Experimental determination of this curve is complicated because it normally occurs at very extreme conditions which can represent up to 5 times the critical temperature and 12 times the critical pressure [31,32]. There has been a literature focus on calculation of the inversion curve by means of EoSs such as cubics or Soft-SAFT EoS for n-alkanes, carbon dioxide, six different natural gas mixtures and gas condensates, among others [33-36]. Moreover the inversion curve has also been previously calculated by means of molecular simulation for carbon dioxide, methane, ethane, butane, nitrogen, argon, oxygen, ethylene, carbon monoxide, a model gas condensate mixture, six different natural gas mixtures and two natural gases, among others [21,23,24,32,34,37-40]. In the present work we also present results for the calculations of the Joule-Thomson inversion curve for the studied n-alkanes through the four aforementioned EoSs.

2. Materials and methods

2.1. Materials

Three different substances are used in the calibration of the differential heat-flux calorimeter, i.e. naphthalene, indium and tin. The provider and purity of these substances along with those of the n-alkanes studied in the present work are presented in Table 1. They were used without further purification. Milli-Q water was also used as reference fluid in the C_p measurements.

Table 1
Chemical sample table.

Chemical Name	Source	Initial Mole Fraction Purity*	Purification Method	Analysis Method*
Indium (shots)	Alfa Aesar	0.999999	none	GDMS[a]
Tin (shots)	Alfa Aesar	0.999999	none	GDMS[a]
Naphthalene (powder)	Sigma-Aldrich	0.998	none	GC[b]
n-hexane	Sigma-Aldrich	0.992	none	GC[b]
n-octane	Sigma-Aldrich	0.994	none	GC[b]
n-decane	Sigma-Aldrich	0.994	none	GC[b]
n-dodecane	Sigma-Aldrich	0.995	none	GC[b]
n-tetradecane	Sigma-Aldrich	> 0.999	none	GC[b]
n-hexadecane	Sigma-Aldrich	0.994	none	GC[b]

*Given by the manufacturer

[a]Glow discharge mass spectrometry

[b]Gas chromatography

2.2. Experimental technique

The experimental technique used to measure the heat capacities is a Calvet type differential heat-flux calorimeter C80 from Setaram, which can operate in both isothermal and differential scanning calorimeter modes. This calorimeter has a Calvet calorimetric detector, in which the sample and reference cells are surrounded completely by a set of 9 concentric rings, each of them containing 38 thermocouples, which allows measuring the total heat transferred by conduction, convection and radiation. The calorimeter can perform measurements from ambient temperature to 573.15 K with a temperature standard uncertainty given by the manufacturer of 0.1 K. The scanning rate can be programmed from 0.001 to 2 $K \cdot min^{-1}$. The conversion of the differential calorimeter detector thermopile signal (E / V) into energy ($\dot{q}$ / W) is performed through an electric calibration by Joule effect from ambient temperature to 573.15 K.

Both the reference and the measurement cells are located in the calorimeter block and can withstand a maximum pressure of 10 MPa. These cells were supplied by Setaram and have an inner volume of approximately 8.5 cm^3. The fluid is filled through the inner of two concentric pipes, which almost reaches the bottom of the cell, whereas the fluid leaves the cell at the top part through the gap between the two concentric pipes. This configuration allows purging the cell when filling the sample, and also facilitates the cleaning procedure.

In order to perform the temperature calibration of the calorimeter the melting points of naphthalene, indium and tin were measured at different scanning rates. Thus, a small amount of these substances was closed inside a glass liner and located in the middle of the measuring cell, in order to do that the measuring cell was filled with alumina powder to approximately 1/3 of its height; similarly the reference cell was also filled with the same quantity of alumina powder. The tests were performed by increasing the temperature from ambient

conditions until a temperature higher than the melting point of these calibration substances at heating rates of 0.01, 0.02, 0.10, 0.20, 0.50, 0.80 and 1.00 K·min^{-1}. The Calisto Acquisition software was used to program the calorimetric experiments and also to obtain the onset temperature of the melting peak, as well as to integrate it.

The schematic of the experimental setup used for the C_p measurement is presented in Figure 1. The sample is filled in the measurement cell of the calorimeter by using a high pressure syringe pump (Teledyne Isco), which is connected to the injection cylinder. This pump uses water as hydraulic fluid, whereas inside the injection cylinder there is a piston which separates the hydraulic fluid from the sample. The pump is also used to keep the pressure constant during the experiments. The pressure during the experiments is measured by means of a pressure transducer Wika S-20, which can measure pressures up to 10 MPa with an standard uncertainty of 0.25% FS. The value of the pressure is recorded every 600 s during the C_p experiments.

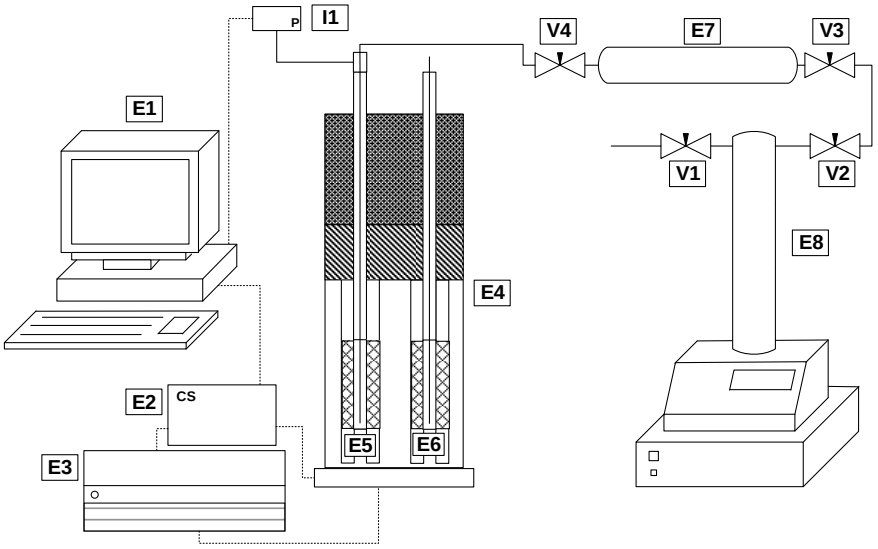

Figure 1. Schematic of the experimental setup. Computer (E1), CS Evolution controller (E2), power module (E3), Setaram C80 calorimeter (E4), measurement cell (E5), reference cell (E6), injection cylinder (E7), syringe pump (E8), high pressure valves (V1 to V4) and pressure transducer (I1).

C_p is obtained in three measurement steps. The reference cell is kept empty in all the three steps whereas the measurement cell is either kept empty or filled with different substances. In the first step, a measurement is made with an empty measurement cell. In the second step, the measurement cell is filled with water, which is used as a reference fluid in this work. In the third step, the measurement cell is filled with the sample whose heat capacity is going to be determined. It is worth mentioning that the last two steps are carried out at constant pressure by connecting the measuring cell to the high-pressure syringe pump running at constant pressure. The mass of the fluid inside the cell at any temperature and pressure conditions is obtained by using literature density values for the sample measured along with the volume of the measuring cell. C_p values of the studied sample can be determined by the following equations, as previously described by Bessières et al. [41]:

$$V_m(T,p) = \frac{\dot{q}_{WE} - \dot{q}_{EE}}{\rho_W(T,p) C_{p,W}(T,p) \frac{dT}{dt}} \quad (1)$$

$$C_{p,S}(T,p) = \frac{\dot{q}_{SE} - \dot{q}_{EE}}{\rho_S(T,p) V_m(T,p) \frac{\mathrm{d}T}{\mathrm{d}t}} \quad (2)$$

where V_m is the volume of the measuring cell, $\dot{q}_{WE}$, $\dot{q}_{SE}$ and $\dot{q}_{EE}$ are the heat flows for the water-empty experiment, the sample-empty experiment and the empty-empty experiment, respectively, ρ_W and ρ_S are the densities of water and of the studied sample, respectively, $C_{p,W}$ and $C_{p,S}$ are the heat capacities at constant pressure of the water and studied sample, respectively, and dT/dt is the scanning rate used, i.e. 0.2 K·min^{-1}. Thus, by knowing both the water density and C_p under the experimental conditions, it is possible to determine the volume of the measuring cell, which together with the density of the studied sample under the same conditions allows quantification of the mass of the studied sample inside the measurement cell and therefore, it is possible to determine the C_p of the studied sample. The water properties were taken from Wagner and Pruss [42], who reported an uncertainty of 0.001% in density and 0.1% in heat capacity. The uncertainty of water density and heat capacity is a main factor affecting the uncertainty of the heat capacity values reported in this work. The density data for the studied samples were taken from Span and Wagner [43] for n-hexane and n-octane, from Lemmon and Span [44] for n-decane, from Lemmon and Huber [45] for n-dodecane, from Khasanshin and Shchemelev [19] for n-tetradecane and from Regueira et al. [46] for n-hexadecane.

The C_p measurements were programed by means of the Calisto Acquisition software. An isothermal zone of at least 7200 s at 303.15 K was set before starting the heating ramp with a rate of 0.2 K·min^{-1} up to 493.15 K. If the boiling point of the studied compound at the experimental pressure was lower than this temperature, then the maximum temperature of the experiment was set around 10 K lower than the boiling point. Once the highest temperature was reached, an isothermal zone was applied for a period of 7200 s at this last temperature. At least two replicates were performed for each experiment and the data reported in this work are the average of the results obtained in the different replicates. The relative expanded C_p uncertainty $U_r(C_p)$ (k=2) is 0.004.

It is important to note that, in order to avoid convection in the system caused by the temperature difference between the fluid in the measurement cell and the fluid in the external pipes, a heating tape was rolled around the external pipes and set to a temperature of 423.15 K or lower than the boiling point of the sample.

2.3. Modelling

In this study two classical cubic EoSs (SRK [27] and PR [28]) and two non-cubic EoSs (PC-SAFT [29] and Soave-BWR [30]) were used to evaluate their performance on the calculation of C_p and Joule-Thomson coefficient of the studied normal alkanes. The two non-cubic models are briefly described below.

2.3.1. PC-SAFT EoS

The PC-SAFT EoS was proposed by Gross and Sadowski [29] to model asymmetric and highly non-ideal systems and it can be expressed in terms of the reduced Helmholtz energy $\tilde{a}$:

$$\tilde{a} = \tilde{a}^{id} + \tilde{a}^{hc} + \tilde{a}^{disp} + \tilde{a}^{assoc} \quad (3)$$

where $\tilde{a}^{id}$ is the ideal gas contribution, $\tilde{a}^{hc}$ is the contribution of the hard-sphere chain reference system, $\tilde{a}^{disp}$ is the dispersion contribution arising from the square well attractive potential and $\tilde{a}^{assoc}$ is the association contribution based on Wertheim's theory [47].

For the hydrocarbon systems consisting only of non-associating components, the $\tilde{a}^{assoc}$ term in Eq. 3 disappears. The remaining three terms have rather complicated forms as compared with SRK or PR.

However, there are only three model parameters for a non-associating component, the chain length *m*, the segment diameter σ and the segment energy ε.
von Solms et al. [48] simplified the original PC-SAFT EoS by assuming that all the segments in the mixture have the same mean diameter *d*, which gives a mixture volume fraction identical to that of the actual mixture.
This variation of PC-SAFT, called the simplified PC-SAFT EoS, is identical to the original PC-SAFT EoS for pure components. For mixtures, the simplified version and the original version are very similar [48]. The simplified version reduces the computation time for non-associating systems and more significantly for associating systems. Therefore, it is more suitable to use the simplified version if the model is considered to be used for reservoir simulation in the future. The simplified version of PC-SAFT is used in our discussion here.

2.3.2. Soave-BWR EoS

The Benedict-Webb-Rubin (BWR) equation of state [49] is a virial type equation of state, and despite its empirical nature, it provides a highly accurate density description compared to many other types of EoS models. The original BWR takes the following functional form:

$$z = \frac{P}{RT\rho} = 1 + B\rho + C\rho^2 + D\rho^5 + E\rho^2(1 + F\rho^2)\exp(-F\rho^2) \tag{4}$$

where ρ is the density, and *B*, *C*, *D*, *E*, and *F* are the five model parameters. A recent modification of the BWR EoS is given by Soave [30]:

$$z = \frac{P}{RT\rho} = 1 + B\rho + D\rho^4 + E\rho^2(1 + F\rho^2)\exp(-F\rho^2) \tag{5}$$

The Soave-BWR EoS used in this study refers to this version of BWR EoS. This EoS has three parameters for each component, T_c, P_c, and ω. Further details about Soave-BWR EoS can be found elsewhere [50].

2.3.3. Isobaric heat capacity calculations

Isobaric heat capacity can be expressed by the following equation:

$$C_p = C_p^{id} + C_p^r \tag{6}$$

This property is evaluated from two independent steps: The ideal gas heat capacity, C_p^{id} which refers to the heat capacity of the free molecule at zero density, and the residual heat capacity, C_p^r which takes into account the intermolecular interactions.
The ideal gas heat capacity term can be calculated by different specific equations and is dependent on temperature only. In this work, the ideal gas heat capacity is calculated from the correlations in DIPPR [51], and the residual part is calculated by means of equations of state. The temperature derivatives of the reduced Helmholtz energy are required in the calculation of the residual part [52]. The following equations show how C_p^r is calculated:

$$F = \frac{A^r(T, V, \boldsymbol{n})}{RT} \tag{7}$$

$$\frac{C_v^r(T, V, \boldsymbol{n})}{R} = -T^2\left(\frac{\partial^2 F}{\partial T^2}\right)_{V,\boldsymbol{n}} - 2T\left(\frac{\partial F}{\partial T}\right)_{V,\boldsymbol{n}} \tag{8}$$

$$\frac{C_p^r}{R} = \frac{C_v^r\left(T,V,\boldsymbol{n}\right)}{R} - \left(\frac{T}{R}\right)\frac{\left(\frac{\partial P}{\partial T}\right)_{V,\boldsymbol{n}}^2}{\left(\frac{\partial P}{\partial V}\right)_{T,\boldsymbol{n}}} - n \tag{9}$$

In these equations, V is the total volume, $\boldsymbol{n}$ is the mole numbers vector, n is the total mole number, A^r is the residual Helmholtz energy, F is the reduced residual Helmholtz function, R is the universal gas constant, and C_v^r is the residual heat capacity at constant volume.

2.3.4. Joule-Thomson coefficient calculations

Joule-Thomson coefficients (μ_{JT}) can be expressed by:

$$\mu_{JT}\left(T,P,\boldsymbol{n}\right) \equiv \left(\frac{\partial T}{\partial P}\right)_{H,\boldsymbol{n}} = -\frac{1}{C_p}\left[V + T\frac{\left(\frac{\partial P}{\partial T}\right)_{V,\boldsymbol{n}}}{\left(\frac{\partial P}{\partial V}\right)_{T,\boldsymbol{n}}}\right] = -\frac{1}{C_p}\left[V - T\left(\frac{\partial V}{\partial T}\right)_{P,\boldsymbol{n}}\right] \tag{10}$$

This last equation was used to calculate the Joule-Thomson coefficient through the different EoSs analyzed in this work. As concerns the calculation of the inversion curve, the pressure was obtained using the bisection method along isotherms until the calculated μ_{JT} was lower than 10^{-5} K·MPa^{-1}.

Critical pressure, critical temperature and acentric factor for SRK, PR, and Soave-BWR EoSs were taken from the DIPPR database, and the model parameters for PC-SAFT were taken from Gross and Sadowski [29]. A summary of these properties is presented in Table 2. It should be mentioned that no volume translation was used for the cubic EoSs in this study and the calculation results are pure predictions of each model.

Table 2
Pure compound parameters for SRK, PR, PC-SAFT and Soave-BWR EoSs.

EoS Parameters	n-hexane	n-octane	n-decane	n-dodecane	n-tetradecane	n-hexadecane
T_c / K*	507.60	568.70	617.70	658.00	693.00	723.00
p_c / MPa*	3.025	2.490	2.110	1.820	1.570	1.400
ω*	0.3013	0.3996	0.4923	0.5764	0.6430	0.7174
σ / Å§	3.7983	3.8373	3.8384	3.8959	3.9396	3.9552
εk^{-1} / K§	236.77	242.78	243.87	249.21	254.21	254.70
m§	3.0576	3.8176	4.6627	5.3060	5.9002	6.6485

*DIPPR database
§Gross and Sadowski

3. Results and discussion

In this section the absolute average deviation (AAD) is employed to compare both the obtained experimental data with calculation results, as well as the obtained experimental data with previously reported literature values. In the first case the following equation is used:

$$AAD/\% = \frac{100}{k}\sum_{i=1}^{k}\left|\frac{Y^{Calc.} - Y^{Exp.}}{Y^{Exp.}}\right| \quad (11)$$

whereas in the second case the following equation is used:

$$AAD/\% = \frac{100}{k}\sum_{i=1}^{k}\left|\frac{Y^{Lit.} - Y^{Exp.}}{Y^{Lit.}}\right| \quad (12)$$

where k is the number of experimental data points, Y stands for the analysed property and *Calc.*, *Exp.* and *Lit.*, stand for calculated, experimental and literature, respectively.

3.1. Calibration

The temperature calibration was performed by measuring the onset melting temperature of 0.1945 g of naphthalene, 0.2903 g of indium and 0.2702 g of tin enclosed in glass liners at different heating rates in the range from 0.01 to 1 K·min^{-1}. These substances were chosen because their melting points cover the working temperature range of the calorimeter. The measured onset melting temperatures increase with the scanning rate and a correction equation for temperature was introduced in the Calisto software to match the melting temperatures reported in the literature, i.e. 353.45 K for naphthalene [53], 429.748 K for indium [54] and 505.078 K for tin [54]. Thus, for a scanning rate of 0.2 K·min^{-1}, which is the rate used in the C_p measurements, a temperature standard uncertainty of 0.2 K was found for the onset melting temperature of the aforementioned substances.

As concerns the enthalpy of melting (ΔH_m), it was obtained for indium and tin through the integration of their melting peaks. The peak integration was performed for all the studied scanning rates finding an absolute average deviation of 1.5% and 1.3% for indium and tin, respectively, when the obtained enthalpy was compared with the values previously reported by Gmelin and Sarge [54].

3.2. Isobaric heat capacity

The volume of the measurement cell was obtained according to Eq. 1 after analysis of the data from the water thermogram at 10 MPa. Two replicates were performed and the average volume was used. It should be mentioned that a slight endothermic effect, attributed to convection caused by the temperature difference between the water in the measurement cell and that in the external pipes, was observed in the water thermogram at temperatures higher than 438.15 K. Thus, a constant volume of the measurement cell equal to that at 438.15 K was assumed at higher temperatures. It was also assumed that the volume of the cells is the same at 0.1 and 10 MPa.

The values obtained for the volume of the measurement cell were used to obtain C_p values of the different n-alkanes studied in this work by means of Eq. 2. These data are presented in table 3, where the average pressure along the experiment is reported. It should be noted that the maximum temperature of the reported data is conditioned either by the alkane bubble point or by the observation of endothermic convection effects in the thermogram.

Table 3

Heat capacity values at constant pressure[a], C_p, of the n-alkanes studied in this work in JK^{-1}g^{-1}.

	p/MPa											
T/K	0.14	10.09	0.10	10.13	0.12	10.17	0.10	10.18	0.12	10.12	0.13	10.09

	n-hexane		n-octane		n-decane		n-dodecane		n-tetradecane		n-hexadecane	
323.15	2.363	2.328	2.305	2.284	2.293	2.270	2.268	2.261	2.266	2.257	2.268	2.262
328.15	2.387	2.349	2.326	2.304	2.307	2.289	2.287	2.278	2.282	2.274	2.284	2.278
333.15	2.412	2.373	2.346	2.325	2.323	2.308	2.306	2.297	2.299	2.291	2.300	2.294
338.15	–	2.392	2.367	2.344	2.342	2.326	2.324	2.315	2.316	2.308	2.317	2.311
343.15	–	2.415	2.387	2.364	2.363	2.345	2.343	2.333	2.334	2.325	2.334	2.325
348.15	–	2.438	2.409	2.384	2.383	2.364	2.362	2.351	2.352	2.343	2.353	2.341
353.15	–	2.459	2.430	2.403	2.403	2.383	2.381	2.369	2.371	2.360	2.369	2.360
358.15	–	2.485	2.452	2.425	2.421	2.404	2.400	2.389	2.390	2.379	2.388	2.378
363.15	–	2.507	2.474	2.444	2.438	2.422	2.419	2.407	2.408	2.397	2.405	2.394
368.15	–	2.534	2.496	2.465	2.458	2.441	2.438	2.426	2.427	2.414	2.423	2.413
373.15	–	–	2.520	2.486	2.479	2.462	2.459	2.443	2.446	2.435	2.443	2.432
378.15	–	–	2.542	2.508	2.499	2.481	2.478	2.462	2.465	2.452	2.461	2.449
383.15	–	–	2.569	2.529	2.520	2.500	2.498	2.481	2.484	2.469	2.480	2.468
388.15	–	–	–	2.547	2.542	2.519	2.517	2.501	2.504	2.486	2.498	2.487
393.15	–	–	–	2.564	2.564	2.540	2.538	2.519	2.521	2.506	2.516	2.505
398.15	–	–	–	2.591	2.585	2.560	2.556	2.543	2.543	2.524	2.535	2.523
403.15	–	–	–	–	2.609	2.580	2.576	2.559	2.562	2.539	2.555	2.542
408.15	–	–	–	–	–	2.601	2.598	2.576	2.583	2.563	2.575	2.561
413.15	–	–	–	–	–	2.620	2.617	2.593	2.600	2.579	2.592	2.581
418.15	–	–	–	–	–	2.641	2.638	2.607	2.619	2.598	2.612	2.601
423.15	–	–	–	–	–	2.666	2.659	2.628	2.638	2.615	2.631	2.619
428.15	–	–	–	–	–	2.689	2.680	2.647	2.657	2.632	2.648	2.634
433.15	–	–	–	–	–	–	2.704	2.667	2.676	2.651	2.667	2.651
438.15	–	–	–	–	–	–	2.732	2.690	2.698	2.668	2.688	2.670
443.15	–	–	–	–	–	–	–	2.713	2.721	2.689	2.708	2.691
448.15	–	–	–	–	–	–	–	2.734	2.740	2.710	2.726	2.710
453.15	–	–	–	–	–	–	–	2.759	2.762	2.730	2.748	2.725
458.15	–	–	–	–	–	–	–	–	2.793	2.751	–	2.744
463.15	–	–	–	–	–	–	–	–	2.821	2.774	–	2.762
468.15	–	–	–	–	–	–	–	–	–	2.792	–	2.783
473.15	–	–	–	–	–	–	–	–	–	2.813	–	2.804
478.15	–	–	–	–	–	–	–	–	–	2.837	–	–
483.15	–	–	–	–	–	–	–	–	–	2.857	–	–

[a]Relative expanded C_p uncertainty $U_r(C_p)$ (k=2): 0.004; standard temperature uncertainty $u(T)$: 0.2 K; standard pressure uncertainty $u(p)$: 0.025 MPa.

Additionally, the experimental heat capacities are depicted in Figure 2 as a function of temperature for the two different pressures that have been studied. It can be observed that C_p increases significantly (up to 24 %) with temperature in the studied temperature range, however the change of this property with pressure is small. C_p decreases with pressure at constant temperature, with a maximum change of 1.7% in the experimental (T,p) range.

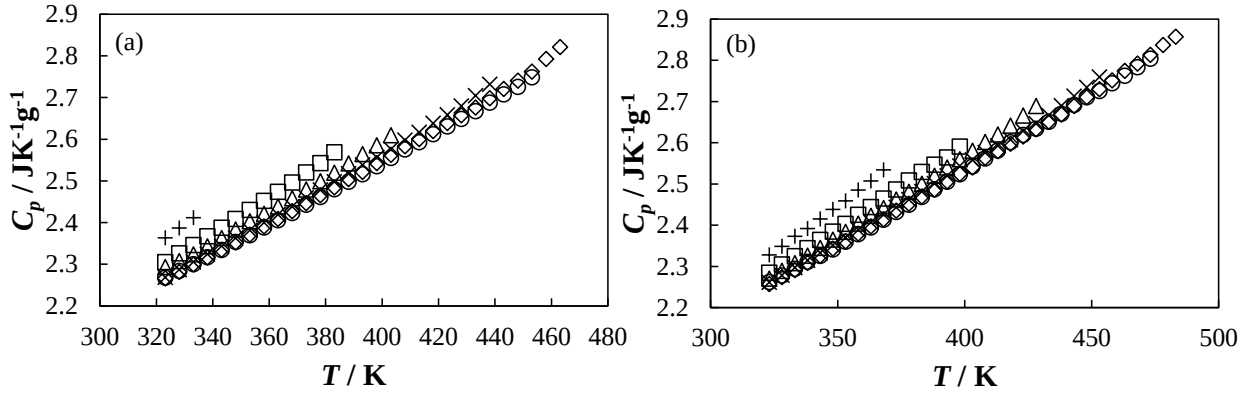

Figure 2. C_p of the n-alkanes as a function of temperature at (a) 0.1 MPa and (b) 10 MPa. n-hexane (+), n-octane (□), n-decane (△), n-dodecane (×), n-tetradecane (◇) and n-hexadecane (○).

The measured values of C_p (Table 3) were compared with existing literature values. As concerns n-hexane, Cerdeiriña et al. [55] published C_p values in the temperature range from (288.15 to 333.15) K at 0.1 MPa, Zaripov et al. [56] reported values in the temperature range from (298.15 to 348.15) K and pressures up to 147 MPa, Bessières et al. [15] measured C_p of this alkane from (313.15 to 373.15) K and pressures up to 100 MPa. Additionally, González-Salgado et al. [1] reported data on C_p of n-hexane from (283.15 to 323.15) K at pressures up to 60 MPa.

As concerns n-octane, Cerdeiriña et al. [55] published values of this property from (288.15 to 333.15) K at 0.1 MPa, Burgdorf et al. [57] at 298.15 K and 323.15 K at 0.1 MPa and Banipal et al. [16] reported C_p data from (313.15 to 373.15) K at pressures up to 60 MPa.

Regarding n-decane Cerdeiriña et al. [58] reported values from (278.15 to 338.15) K at 0.1 MPa, Gates et al. [59] measured C_p values from (298.15 to 368.15) K at 0.1 MPa. Páramo et al. [2] and Schlinger and Sage [60] published saturation heat capacities in the temperature ranges from (278.15 to 348.15) K and (299.82 to 366.48) K, respectively. Moreover, Banipal et al. [16] reported values of this property from (318.15 to 373.15) K up to 10 MPa, González-Salgado et al. [1] determined this property of n-decane from (283.15 to 323.15) K up to 60 MPa and Bessières et al. [17] measured n-decane heat capacities from (302.80 to 373.27) K at 0.1 and 10 MPa.

Concerning n-dodecane, Cerdeiriña et al. [55] published C_p data from (283.15 to 333.15) K at 0.1 MPa, whereas Burgdorf et al. [57] at 298.15 K and 323.15 K at 0.1 MPa. Salvetti et al. [61] published a correlation for the experimental C_p data measured from (293 to 370) K at 0.1 MPa. Besides, Páramo et al. [2] reported saturation heat capacity from (278.15 to 338.15) K. As for higher pressures, Bessières et al. [4] measured C_p values in the temperature range from (313.15 to 373.15) K up to 100 MPa, whereas Khasanshin et al. [18] reported values of this property from (293 to 433) K up to 140 MPa calculated using as input experimental data on speed of sound as a function of temperature and pressure and C_p and density at atmospheric pressure. Also, González-Salgado et al. [1] determined this property of n-dodecane from (283.15 to 323.15) K up to 60 MPa.

As regards n-tetradecane, González-Salgado et al. [1] determined C_p of this alkane from (283.15 to 323.15) K up to 60 MPa, whereas Khasanshin et al. [19] published values of this property from (293 to 433) K up to 140 MPa calculated using as input experimental data on speed of sound as a function of temperature and pressure and C_p and density at atmospheric pressure.

Finally, as for n-hexadecane, Cerdeiriña et al. [55] measured this property in the temperature range from (308.15 to 333.15) K at 0.1 MPa, whereas Banipal et al. [16] reported C_p in the temperature range from (318.15 to 373.15) K up to 10 MPa.

Moreover, the C_p values reported in the present work have been also compared with data obtained from the correlations provided by Zábranský et al. [9] and Růžička et al. [6], as well as data obtained through the EoSs by Span and Wagner [43], Lemmon and Span [44] and Lemmon and Huber [45].

The relative deviations between the C_p data reported in this work and all the aforementioned literature data are plotted in Figure 3. It can be observed that the agreement with most of the previously reported data is within 1.0 %. However it has been found a high deviation for n-hexadecane at 0.1 MPa and temperatures higher than 400 K with data reported by Zábranský et al. [9] and by Petit and Minassian [14], one explanation for this deviation could be that the uncertainty of the reported data at temperatures higher than 350 K is described as low reliability (uncertainty up to 3%) by Zábranský et al. [9], moreover the correlation provided by these last authors is based only on the experimental data by Petit and Minassian [14] at temperatures higher than 373.1 K. As concerns the AADs, values of 0.38 %, 0.69 %, 0.59 %, 0.80%, 0.34 % and 0.79 % were found for n-hexane, n-octane, n-decane, n-dodecane, n-tetradecane and n-hexadecane, respectively.

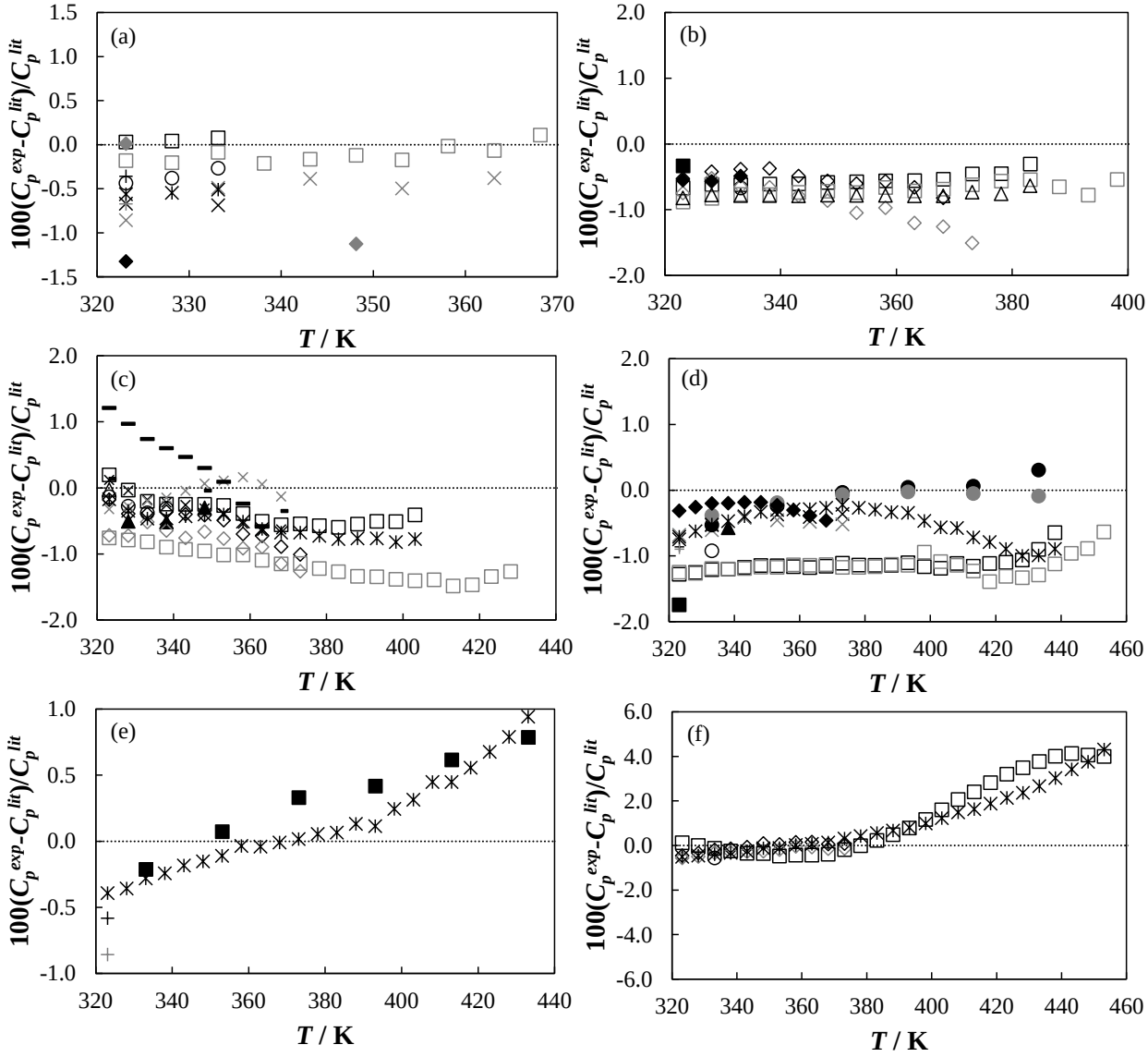

Figure 3. Relative deviation between C_p values obtained in this work (C_p^{exp}) and those from literature (C_p^{lit}) for (a) n-hexane [Zaripov et al. [56] (◆), Bessières et al. [15] (×), Cerdeiriña et al. [55] (○), González-Salgado et al. [1] (+), Zábranský et al. [9] (∗), Span and Wagner [43] (□)]; (b) n-octane [Banipal et al. [16] (◇), Cerdeiriña et al. [55] (○), Růžička et al. [6] (△), Span and Wagner [43] (□), Burgdorf et al. [57] (■), Coulier et al. [62] (◆)]; (c) n-decane [Gates et al. [59] (-), Banipal et al. [16] (◇), Páramo et al. [2] (▲), Bessières et al. [17] (×), González-Salgado et al. [1] (△), Cerdeiriña et al. [58] (○), Schlinger and Sage [60] (—), Zábranský et al. [9] (∗), Lemmon and Span [44] (□)]; (d) n-dodecane [Cerdeiriña et al. [55] (○), Páramo et al. [2] (▲), Bessières et al. [4] (×), Khasanshin et al. [18] (●), González-Salgado et al. [1] (+), Burgdorf et al. [57] (■), Salvetti et al. [61] (◆), Zábranský et al. [9] (∗), Lemmon and Huber [45] (□)]; (e) n-tetradecane [González-Salgado et al. [1] (+), Khasanshin et al. [19] (■), Zábranský et al. [9] (∗)] and (f) n-hexadecane [Banipal et al. [16] (◇), Cerdeiriña et al. [55] (○), Petit and Minassian [14] (□), Zábranský et al. [9] (∗)]. Black symbols represent data at 0.1 MPa and grey symbols represent data at 10 MPa.

The calculation results for C_p using all the four EoSs are presented in Tables A.1 to A.4 in the supplementary material. The Absolute Average Deviation (AAD) and maximum deviation obtained in the calculation of C_p of the n-alkanes at 0.1 and 10 MPa using the different EoSs described in section 2.3 are summarized in Table 4. The results show that both the AAD and maximum deviation are lower for the non-cubic EoSs than for the cubic models. PR, with AAD around 3%, gives the largest deviation among all the four analysed EoSs, while PC-SAFT has the lowest AAD (0.27%) for both low and high pressures. Soave-BWR gives almost similar average deviation as PC-SAFT for 0.1 MPa but a slightly higher deviation for 10 MPa. In general, the model performance at 10 MPa and 0.1 MPa are very similar. The maximum deviation for PR is 6.65% for n-hexadecane at 10 MPa, while for PC-SAFT the maximum deviation is 1.13% for n-tetradecane at 0.1 MPa. The overall AAD for all the n-alkanes tested is presented in Figure 4.

Table 4
Absolute Average Deviation (AAD) and maximum deviation (Max. Dev.) in the C_p calculation of the n-alkanes studied in this work at 0.1 and 10 MPa using different EoSs.

	SRK		PR		PC-SAFT		Soave-BWR	
p/MPa	0.1	10	0.1	10	0.1	10	0.1	10
	n-hexane							
AAD / %	0.14	0.34	2.18	2.10	0.13	0.35	0.76	0.92
Max. Dev. / %	0.22	0.89	2.42	2.93	0.15	0.44	0.77	1.03
	n-octane							
AAD / %	0.66	0.88	2.39	2.55	0.07	0.27	0.63	0.78
Max. Dev. / %	1.62	1.99	3.72	3.96	0.13	0.47	0.77	1.10
	n-decane							
AAD / %	1.12	1.29	2.91	2.90	0.19	0.25	0.37	0.43
Max. Dev. / %	2.97	2.86	5.02	4.80	0.34	0.39	0.61	0.58
	n-dodecane							
AAD / %	1.31	1.61	3.03	3.18	0.31	0.27	0.16	0.21
Max. Dev. / %	2.81	3.19	4.82	5.11	0.89	0.91	0.66	0.68
	n-tetradecane							
AAD / %	1.37	1.51	3.02	3.01	0.29	0.19	0.18	0.32
Max. Dev. / %	3.84	4.04	5.81	5.94	1.13	0.87	0.88	0.60
	n-hexadecane							
AAD / %	1.91	2.05	3.60	3.61	0.39	0.32	0.18	0.25
Max. Dev. / %	4.50	4.71	6.49	6.65	0.82	0.67	0.71	0.91
	Overall							

AAD / %	1.33	1.46	3.05	3.04	0.27	0.27	0.27	0.40

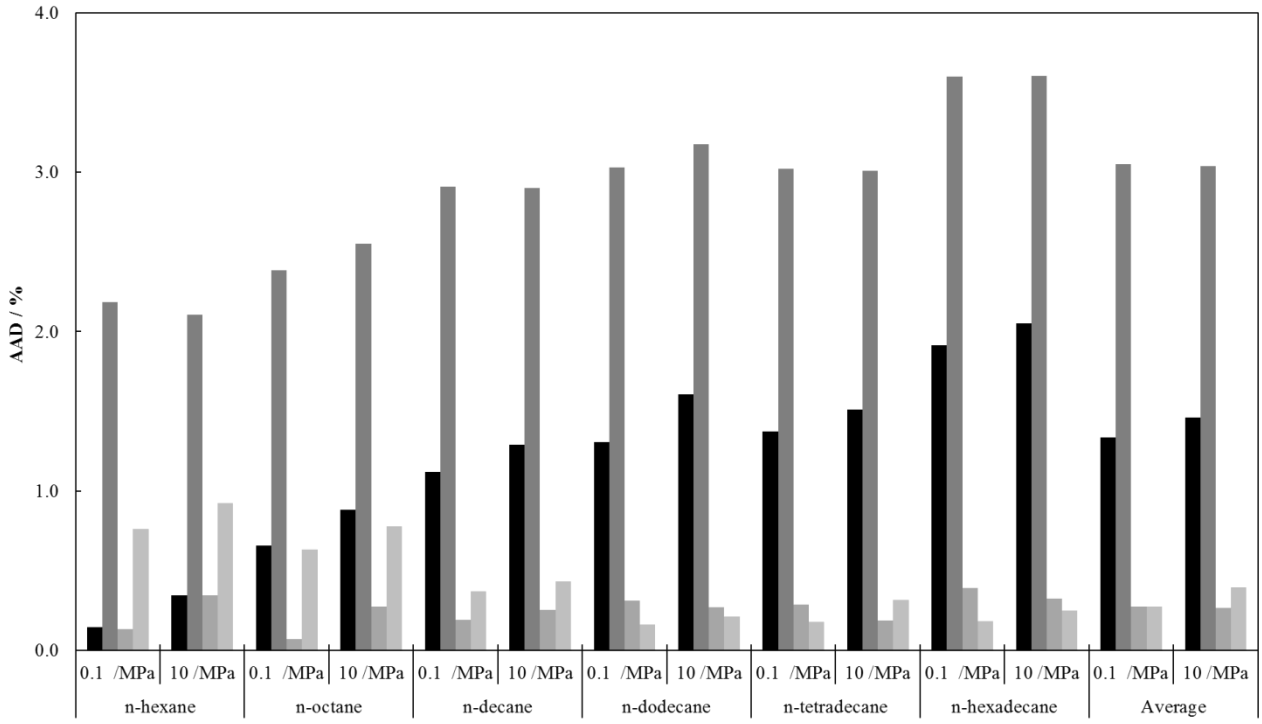

Figure 4. Absolute Average Deviation (AAD) in calculation of C_p of the n-alkanes studied in this work using different EoSs at 0.1 MPa and 10 MPa. SRK (■), PR (■), PC-SAFT (■) and Soave-BWR (■).

In order to see the trend of the specific C_p with the carbon number of the n-alkanes, we have plotted in Figure 5 the experimental C_p as well as the model predictions as a function of the carbon number at 0.1 and 10 MPa at four different temperatures. In general, it can be observed that the specific C_p decreases with carbon number until carbon number 10 or 12, and keeps almost constant for higher carbon numbers. This behaviour has been already reported by Huang et al. [63]. Concerning model predictions, as it can be seen in Figure 5, SRK and PR under predict C_p values for all the n-alkanes and the deviation increases as the carbon number increases. PC-SAFT and Soave-BWR give better prediction of C_p as a function of carbon number at both 0.1 and 10 MPa.

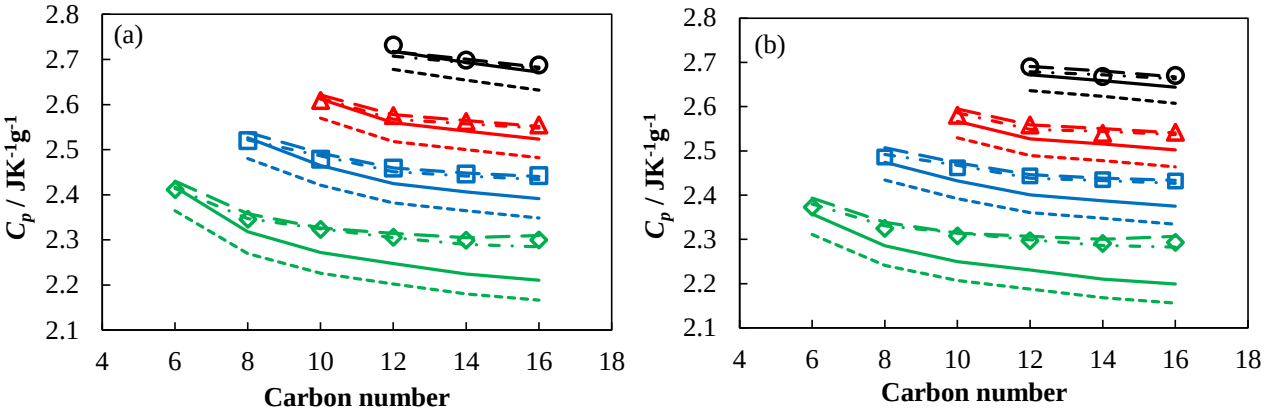

Figure 5. C_p of n-alkanes as a function of the carbon number at (a) 0.1 MPa and at (b) 10 MPa. 333.15 K (◇), 373.15 K (□), 403.15 K (△) and 438.15 K (○). SRK (solid line), PR (dashed line), PC-SAFT (dash-dot line) and Soave-BWR (long dashed line).

In order to get a deeper understanding on how the models predict the values of C_p with carbon number, the model predictions using SRK, PR and PC-SAFT for heavier normal alkanes up to n-C_{36} are presented in Figure 6. The results show that these three EoSs tend to approach a constant value for the specific C_p as the carbon number increases. For Soave-BWR, on the other hand, the predictions for normal alkanes heavier than n-hexadecane seem to be unreliable as the values of specific heat capacities increase with carbon number.

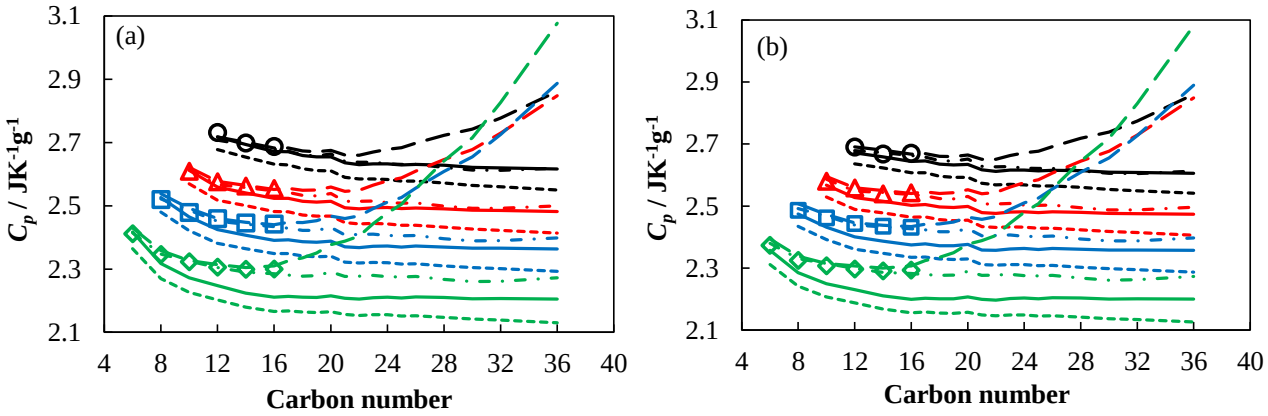

Figure 6. C_p of n-alkanes up to n-C_{36} as a function of the carbon number at (a) 0.1 MPa and at (b) 10 MPa. 333.15 K (◇), 373.15 K (□), 403.15 K (△) and 438.15 K (○). SRK (solid line), PR (dashed line), PC-SAFT (dash-dot line) and Soave-BWR (long dashed line).

The behaviour of the molar heat capacity as a function of temperature and carbon number was also analysed (Figure 7). The molar heat capacity of the studied n-alkanes at constant pressure increases linearly with the carbon number from 6 to 16, showing that the -(CH_2)- group gives approximately the same contribution to the heat capacity of n-alkanes, which is less apparent in Figure 6 for specific heat capacity. But it can still be observed that as the carbon number increases, the contribution of the -CH_2- groups becomes more dominant relative to that of the –CH_3 group and the specific heat capacity becomes almost constant.

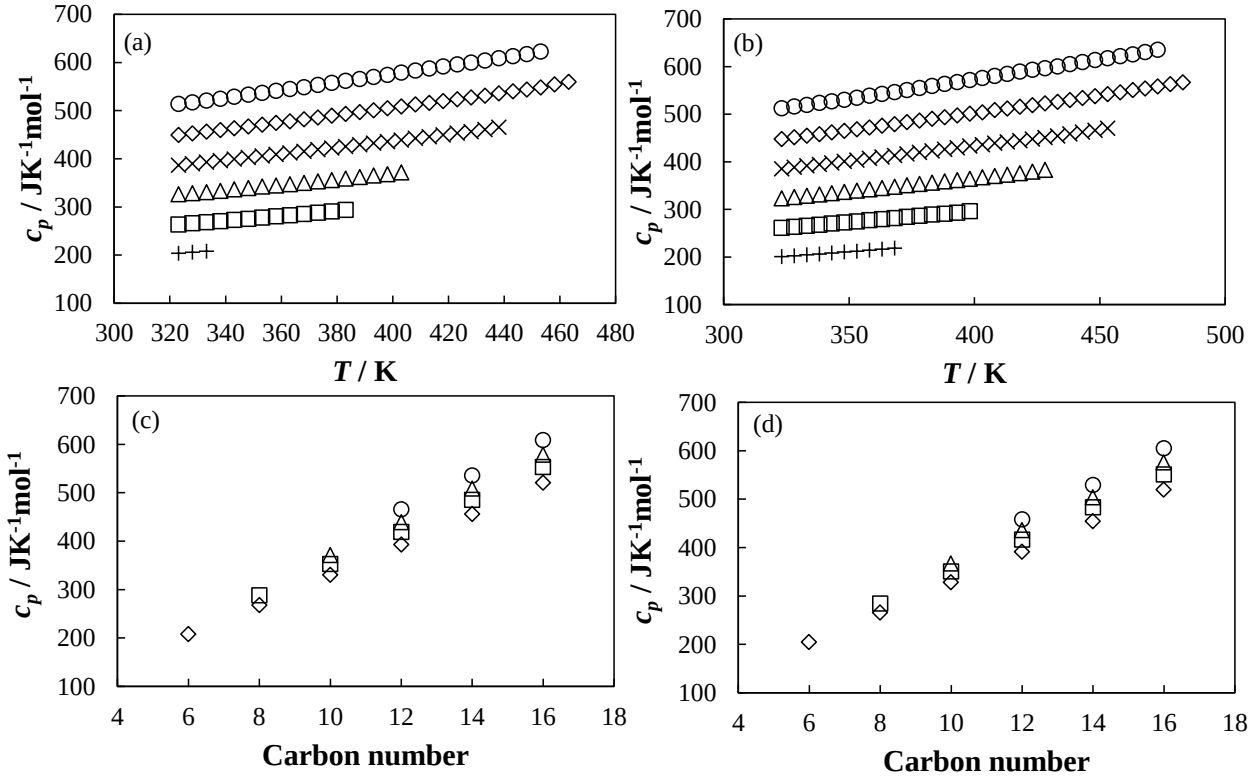

Figure 7. Molar heat capacity of n-alkanes at constant pressure as a function of temperature and carbon number at (a, c) 0.1 MPa and at (b, d) 10 MPa. (a, b): n-hexane (+), n-octane (□), n-decane (△), n-dodecane (×), n-tetradecane (◇) and n-hexadecane (○); (c, d): 333.15 K (◇), 373.15 K (□), 403.15 K (△) and 438.15 K (○).

We have correlated the molar heat capacity as a function of temperature and carbon number (N_c) according to the following equation:

$$c_p / JK^{-1}mol^{-1} = a + b \cdot N_c + c \cdot (T/K) + d \cdot N_c \cdot (T/K) \quad (14)$$

where c_p is the molar heat capacity at constant pressure, T is the temperature, N_c is the carbon number and a, b, c and d are fitting parameters for the experimental data presented in this work. The fitting parameters are summarized in Table 5.

Table 5
Fitting parameters and absolute average deviation of the fit of the experimental molar heat capacity (JK^{-1}mol^{-1}) of the n-alkanes measured in this work (Fig. 7 (a, b)) as a function of temperature and carbon number (Eq. (14)).

p/MPa	a / JK^{-1}mol^{-1}	b / JK^{-1}mol^{-1}	c / JK^{-2}mol^{-1}	d / JK^{-2}mol^{-1}	AAD / %
0.10	-7.293	15.02	0.0755	0.0488	0.2
10.0	-4.451	15.27	0.0595	0.0482	0.2

3.3. Joule-Thomson coefficient

The Joule-Thomson coefficient (μ_{JT}) was obtained from the experimental C_p data by use of the following equation, which is equivalent to Eq. 10:

$$\mu_{JT}(T,p) = \frac{1}{\rho(T,p)C_p(T,p)}\left(T\alpha_p(T,p) - 1\right) \quad (15)$$

where $\rho(T,p)$ is the density of the n-alkane, $C_p(T,p)$ is its isobaric heat capacity and $\alpha_p(T,p)$ is the isobaric thermal expansion coefficient.

The same density data which were used to obtain the C_p values are used in Eq. 15 to obtain the Joule-Thomson coefficient, that is, densities from Span and Wagner [43] for n-hexane and n-octane, from Lemmon and Span [44] for n-decane, from Lemmon and Huber [45] for n-dodecane, from Khasanshin and Shchemelev [19] for n-tetradecane and from Regueira et al. [46] for n-hexadecane. As concerns the isobaric thermal expansion coefficient, the values of this property for the studied n-alkanes were obtained by cubic fitting of the aforementioned literature density data as a function temperature at 0.1 and 10 MPa and subsequent differentiation of the obtained fits with respect to temperature. The relative expanded μ_{JT} uncertainty $U_r(\mu_{JT})$ (k=2) is estimated to be lower or equal to 0.009 for n-hexane, n-octane, n-decane, n-dodecane and n-tetradecane and lower or equal to 0.016 for n-hexadecane. The values of the Joule-Thomson coefficient are presented in Table 6. Moreover the obtained values of this property are plotted against temperature in Figure 8. It can be observed that the values of this property are negative for all the studied n-alkanes ranging from -0.42 to -0.23 K·MPa^{-1} and they become more negative with increasing pressure, whereas they increase with temperature. Additionally this property decreases when increasing the alkyl chain length of the n-alkane from n-hexane to n-tetradecane, whereas for n-tetradecane and n-hexadecane very similar values were found, which represents a similar trend of the Joule-Thomson coefficient and specific C_p with alkyl chain length.

Table 6

Joule-Thomson coefficient of the studied n-alkanes[a], μ_{JT}, in K·MPa^{-1} obtained by using Eq. 15.

	p/MPa											
T/K	0.14	10.09	0.10	10.13	0.12	10.17	0.10	10.18	0.12	10.12	0.13	10.09
	n-hexane		n-octane		n-decane		n-dodecane		n-tetradecane		n-hexadecane	
323.15	-0.341	-0.380	-0.390	-0.411	-0.397	-0.413	-0.407	-0.418	-0.412	-0.423	-0.410	-0.419
328.15	-0.329	-0.371	-0.382	-0.404	-0.392	-0.407	-0.402	-0.413	-0.406	-0.417	-0.405	-0.415
333.15	-0.317	-0.362	-0.374	-0.397	-0.386	-0.402	-0.396	-0.408	-0.401	-0.412	-0.399	-0.411
338.15	–	-0.353	-0.365	-0.391	-0.380	-0.397	-0.391	-0.404	-0.396	-0.407	-0.394	-0.407
343.15	–	-0.344	-0.357	-0.384	-0.373	-0.391	-0.385	-0.399	-0.390	-0.402	-0.388	-0.403
348.15	–	-0.334	-0.348	-0.378	-0.366	-0.386	-0.379	-0.394	-0.384	-0.397	-0.382	-0.399
353.15	–	-0.324	-0.339	-0.371	-0.359	-0.380	-0.373	-0.389	-0.379	-0.392	-0.377	-0.395
358.15	–	-0.314	-0.330	-0.364	-0.352	-0.374	-0.368	-0.384	-0.373	-0.386	-0.371	-0.390
363.15	–	-0.303	-0.320	-0.357	-0.346	-0.369	-0.361	-0.379	-0.367	-0.381	-0.366	-0.386
368.15	–	-0.292	-0.310	-0.350	-0.338	-0.363	-0.355	-0.374	-0.361	-0.376	-0.360	-0.382
373.15	–	–	-0.300	-0.342	-0.331	-0.357	-0.348	-0.369	-0.355	-0.371	-0.355	-0.377
378.15	–	–	-0.290	-0.334	-0.323	-0.351	-0.342	-0.363	-0.349	-0.366	-0.349	-0.373
383.15	–	–	-0.279	-0.327	-0.315	-0.345	-0.335	-0.358	-0.343	-0.361	-0.344	-0.368
388.15	–	–	–	-0.319	-0.307	-0.339	-0.328	-0.353	-0.337	-0.357	-0.338	-0.364

393.15	–	–	–	-0.312	-0.298	-0.333	-0.321	-0.347	-0.331	-0.352	-0.333	-0.359
398.15	–	–	–	-0.303	-0.290	-0.327	-0.314	-0.341	-0.325	-0.347	-0.328	-0.354
403.15	–	–	–	–	-0.281	-0.321	-0.307	-0.336	-0.319	-0.343	-0.322	-0.350
408.15	–	–	–	–	–	-0.314	-0.299	-0.331	-0.313	-0.338	-0.317	-0.345
413.15	–	–	–	–	–	-0.308	-0.291	-0.325	-0.307	-0.333	-0.312	-0.340
418.15	–	–	–	–	–	-0.301	-0.283	-0.320	-0.300	-0.329	-0.307	-0.335
423.15	–	–	–	–	–	-0.294	-0.275	-0.314	-0.294	-0.325	-0.302	-0.330
428.15	–	–	–	–	–	-0.287	-0.267	-0.308	-0.287	-0.321	-0.297	-0.325
433.15	–	–	–	–	–	–	-0.257	-0.302	-0.281	-0.316	-0.293	-0.320
438.15	–	–	–	–	–	–	-0.248	-0.295	-0.274	-0.312	-0.288	-0.315
443.15	–	–	–	–	–	–	–	-0.289	-0.267	-0.308	-0.283	-0.310
448.15	–	–	–	–	–	–	–	-0.282	-0.260	-0.304	-0.278	-0.304
453.15	–	–	–	–	–	–	–	-0.275	-0.253	-0.299	-0.274	-0.299
458.15	–	–	–	–	–	–	–	–	-0.245	-0.295	–	-0.294
463.15	–	–	–	–	–	–	–	–	-0.237	-0.291	–	-0.288
468.15	–	–	–	–	–	–	–	–	–	-0.287	–	-0.282
473.15	–	–	–	–	–	–	–	–	–	-0.283	–	-0.276
478.15	–	–	–	–	–	–	–	–	–	-0.279	–	–
483.15	–	–	–	–	–	–	–	–	–	-0.276	–	–

[a]Relative expanded μ_{JT} uncertainty $U_r(\mu_{JT})$ (k=2): 0.009 for n-hexane, n-octane, n-decane, n-dodecane and n-tetradecane and 0.016 for n-hexadecane; standard temperature uncertainty $u(T)$: 0.2 K; standard pressure uncertainty $u(p)$: 0.025 MPa.

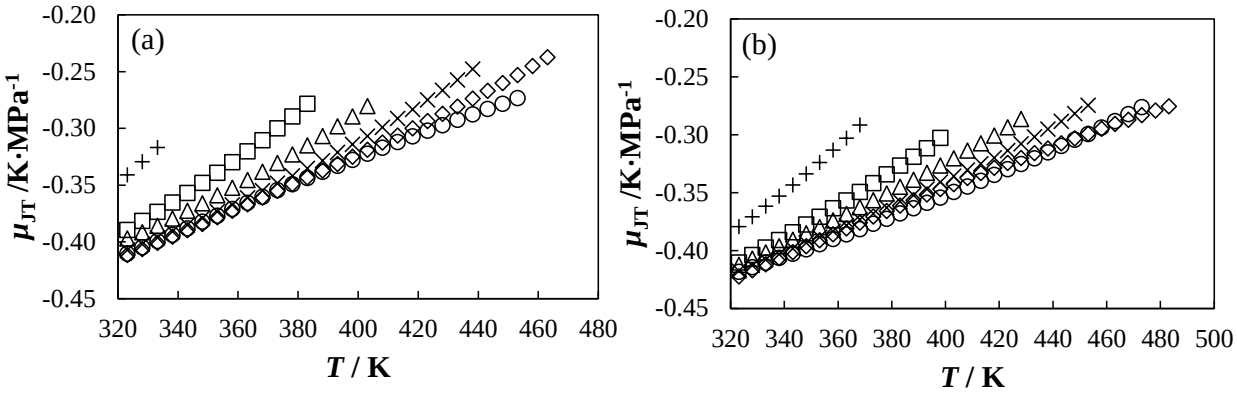

Figure 8. Joule-Thomson coefficient of the n-alkanes as a function of temperature at (a) 0.1 MPa and (b) 10 MPa. n-hexane (+), n-octane (□), n-decane (△), n-dodecane (×), n-tetradecane (◇) and n-hexadecane (○).

The obtained values of the Joule-Thomson coefficient were compared with the values generated by REFPROP of NIST [64], where published n-hexane and n-octane were calculated by the reference EoS of Span and Wagner [43], n-decane by the EoS of Lemmon and Span [44] and n-dodecane by the EoS of Lemmon and Huber [45]. The relative deviations are depicted in Figure 9, where it can be observed that maximum deviations of 1.6 % were found in the comparison of this property with literature data. A global AAD of 0.7 % was obtained in this comparison.

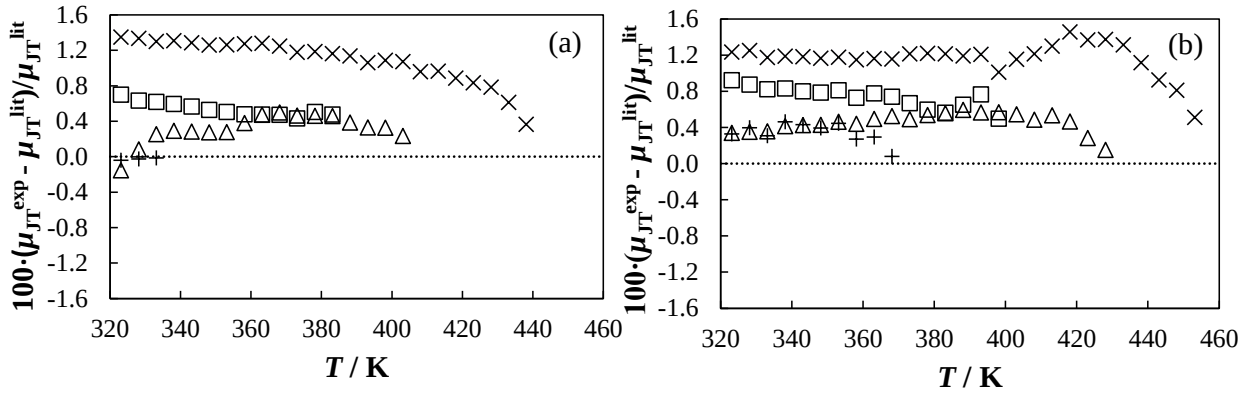

Figure 9. Relative deviation between the Joule-Thomson coefficient values obtained in this work (μ_{JT}^{exp}) and those from literature (μ_{JT}^{lit}) at (a) 0.1 MPa and (b) 10 MPa. n-hexane [43] (+), n-octane [43] (□), n-decane [44] (△) and n-dodecane [45] (×).

The calculation results for Joule-Thomson coefficient using all the four EoSs are presented in Tables A.5 to A.8 in the supplementary material. Table 7 summarizes the Absolute Average Deviation (AAD / %) and the maximum deviation in the calculation of the Joule-Thomson coefficient of the n-alkanes at different pressures using the different EoSs.

Table 7
Absolute Average Deviation (AAD) and maximum deviation (Max. Dev.) in the Joule-Thomson coefficient calculation of the n-alkanes studied in this work at different pressures using different EoSs.

	SRK		PR		PC-SAFT		Soave-BWR	
p/MPa	0.1	10	0.1	10	0.1	10	0.1	10
	n-hexane							
AAD / %	9.11	16.65	3.30	6.97	4.65	3.90	3.09	3.26
Max. Dev. / %	11.30	20.82	5.14	11.35	4.83	4.33	3.29	3.69
	n-octane							
AAD / %	19.71	27.75	12.46	2.55	2.17	1.62	4.10	3.71
Max. Dev. / %	27.64	32.26	19.09	3.96	2.52	1.95	5.15	4.74
	n-decane							
AAD / %	34.37	39.55	25.38	27.95	2.59	2.22	1.49	1.30
Max. Dev. / %	41.87	44.33	31.70	32.85	2.97	2.50	1.82	1.84
	n-dodecane							
AAD / %	42.95	48.43	33.14	35.98	3.90	3.33	0.89	0.48
Max. Dev. / %	49.74	52.20	38.63	39.99	6.80	5.38	2.55	1.75
	n-tetradecane							
AAD / %	54.21	57.97	43.29	44.52	4.02	2.33	3.84	2.93
Max. Dev. / %	61.03	62.23	48.80	49.11	5.57	3.91	5.68	4.42
	n-hexadecane							
AAD / %	65.04	66.91	52.79	52.80	5.05	3.57	5.40	4.68
Max. Dev. / %	69.29	70.79	56.28	56.97	6.74	7.23	7.30	9.40
	Overall							

AAD / %	46.25	48.75	36.10	36.24	3.83	2.81	3.24	2.70

The results show that both the AAD and maximum deviation are significantly lower for the non-cubic EoSs in comparison to the cubic models for the n-alkanes tested in this study. SRK with around 46% deviation, gives the largest deviation among all the four EoSs, while Soave-BWR gives the lowest deviation for both low and high pressures which is 3.24 % and 2.70 %, respectively. PC-SAFT gives slightly higher absolute average deviation than Soave-BWR for both 0.1 MPa and 10 MPa. The maximum AAD for SRK is 70.79% for n-hexadecane at 10 MPa, while for Soave-BWR the maximum AAD is 9.40% for n-hexadecane at 10 MPa. The maximum AAD for PC-SAFT is lower than the other three EoSs. The overall AAD for all the n-alkanes tested is presented in Figure 10.

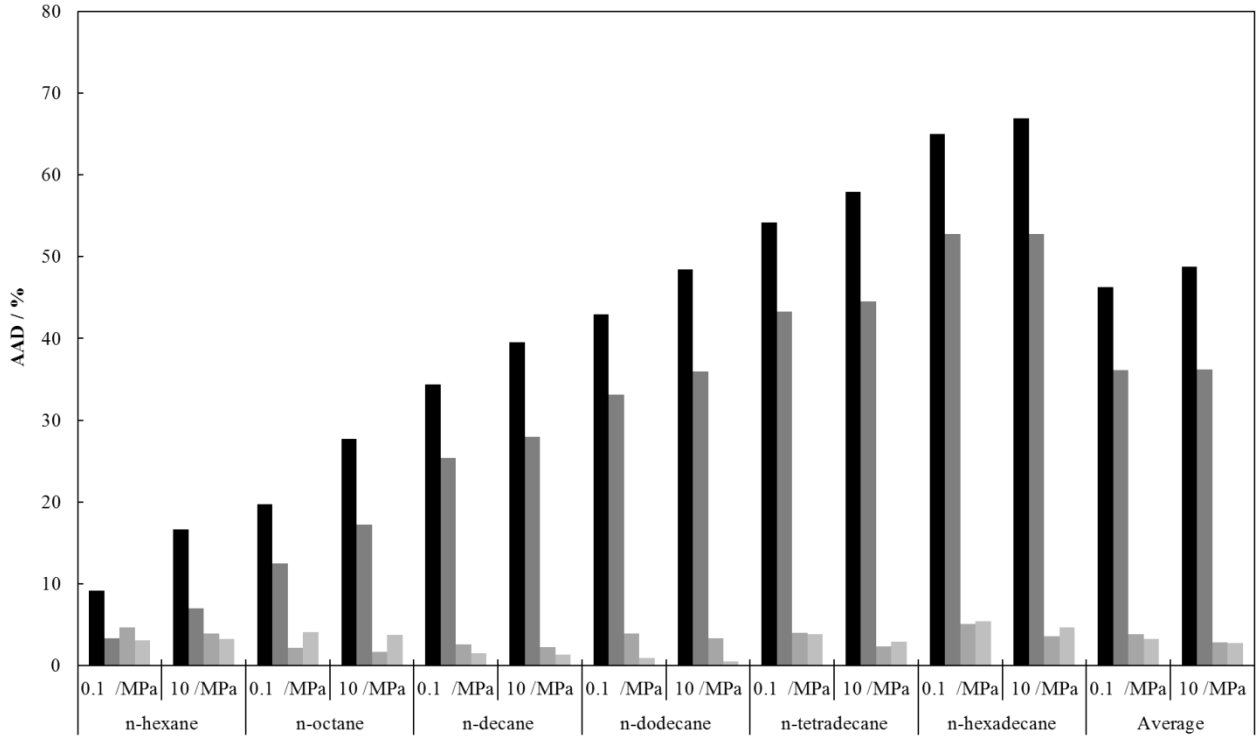

Figure 10. Absolute Average Deviation (AAD) in the calculation of the Joule-Thomson coefficient of the n-alkanes studied in this work using different EoSs at 0.1 MPa and 10 MPa. SRK (■), PR (■), PC-SAFT (■) and Soave-BWR (■).

Figure 11 illustrates the experimental Joule-Thomson coefficient as well as the model predictions as a function of the carbon number at 0.1 and 10 MPa. Both SRK and PR show large deviations and, for clarity, their results are only presented at 333.15 K. SRK and PR under predict the Joule-Thomson coefficient for all the n-alkanes and the deviation increases as the carbon number and pressure increase. PC-SAFT and Soave-BWR give better prediction of Joule-Thomson coefficient as a function of carbon number at both 0.1 and 10 MPa.

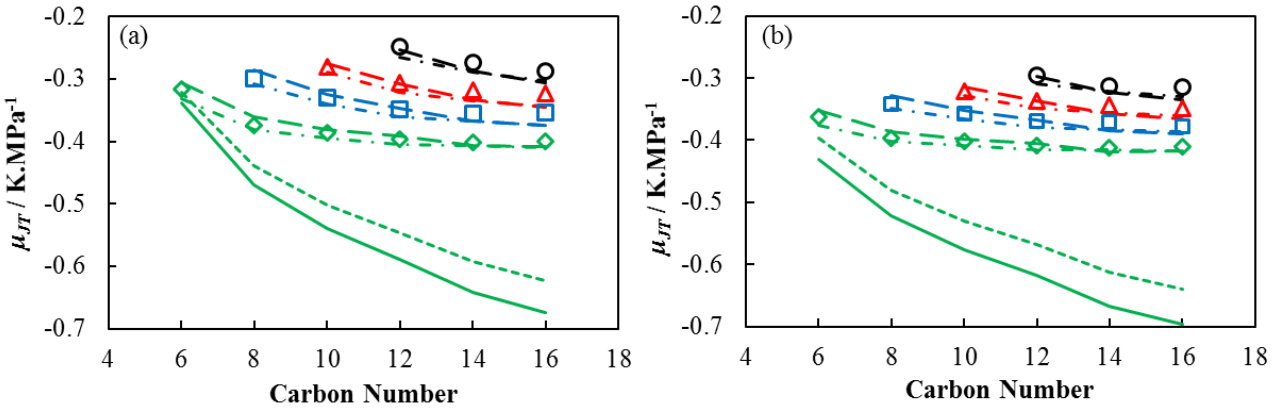

Figure 11. Joule-Thomson coefficient of n-alkanes as a function of the carbon number at (a) 0.1 MPa and at (b) 10 MPa. 333.15 K (◇), 373.15 K (□), 403.15 K (△) and 438.15 K (○). SRK (solid line), PR (dashed line), PC-SAFT (dash-dot line) and Soave-BWR (long dashed line).

Both for PC-SAFT and Soave-BWR we have further investigate the prediction capability of the Joule-Thomson coefficient of heavier n-alkanes, which is shown in Figure 12. It can be observed that both models give similar predictions at high temperatures. It is also interesting to note that both models predict an increase in μ_{JT} with carbon number, this increase happens for carbon numbers higher than n-C_{32} for PC-SAFT, whereas for Soave-BWR μ_{JT} increases for carbon numbers higher than n-C_{16} at low temperatures.

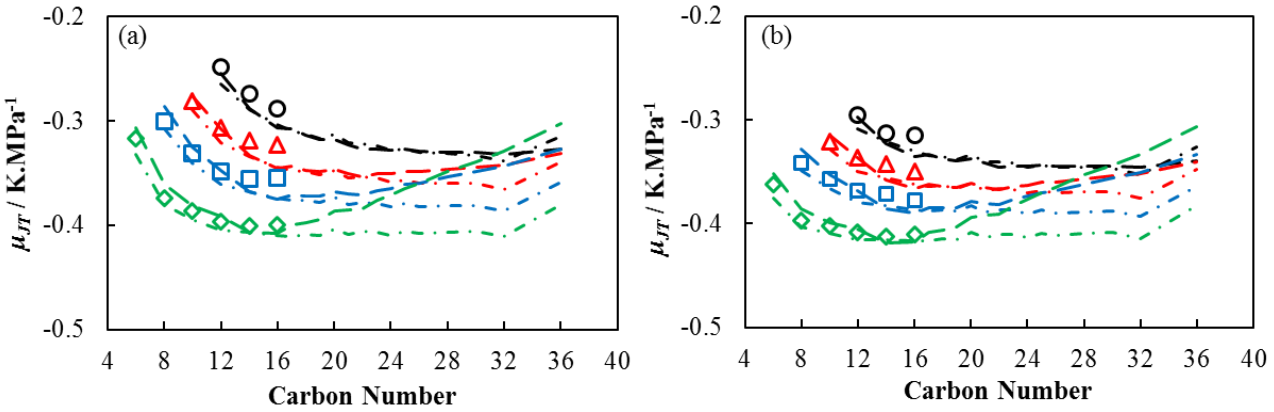

Figure 12. Joule-Thomson coefficient of n-alkanes up to n-C_{36} as a function of the carbon number at (a) 0.1 MPa and at (b) 10 MPa. 333.15 K (◇), 373.15 K (□), 403.15 K (△) and 438.15 K (○). PC-SAFT (dash-dot line) and Soave-BWR (long dashed line).

As concerns the calculation of the Joule-Thomson inversion curve through the four different EoSs studied in this work, the inversion curves of methane, ethane and propane were first calculated, as there are available experimental data [21,65] for these light alkanes. The obtained results are depicted in Figure 13, so that it is possible to see the performance of the different EoSs for the prediction of the experimental data. It can be observed that the best prediction for the inversion curve is obtained by Soave-BWR for ethane and propane, whereas SRK gives the best predictions for methane. Moreover, the studied models have a better agreement in the low-temperature branch, whereas noticeable differences occur in the high-temperature branch for these three n-alkanes. As previously stated by Colina et al. [35], this is because the Joule-Thomson coefficients are more sensitive to pressure and temperature in the high-temperature branch.

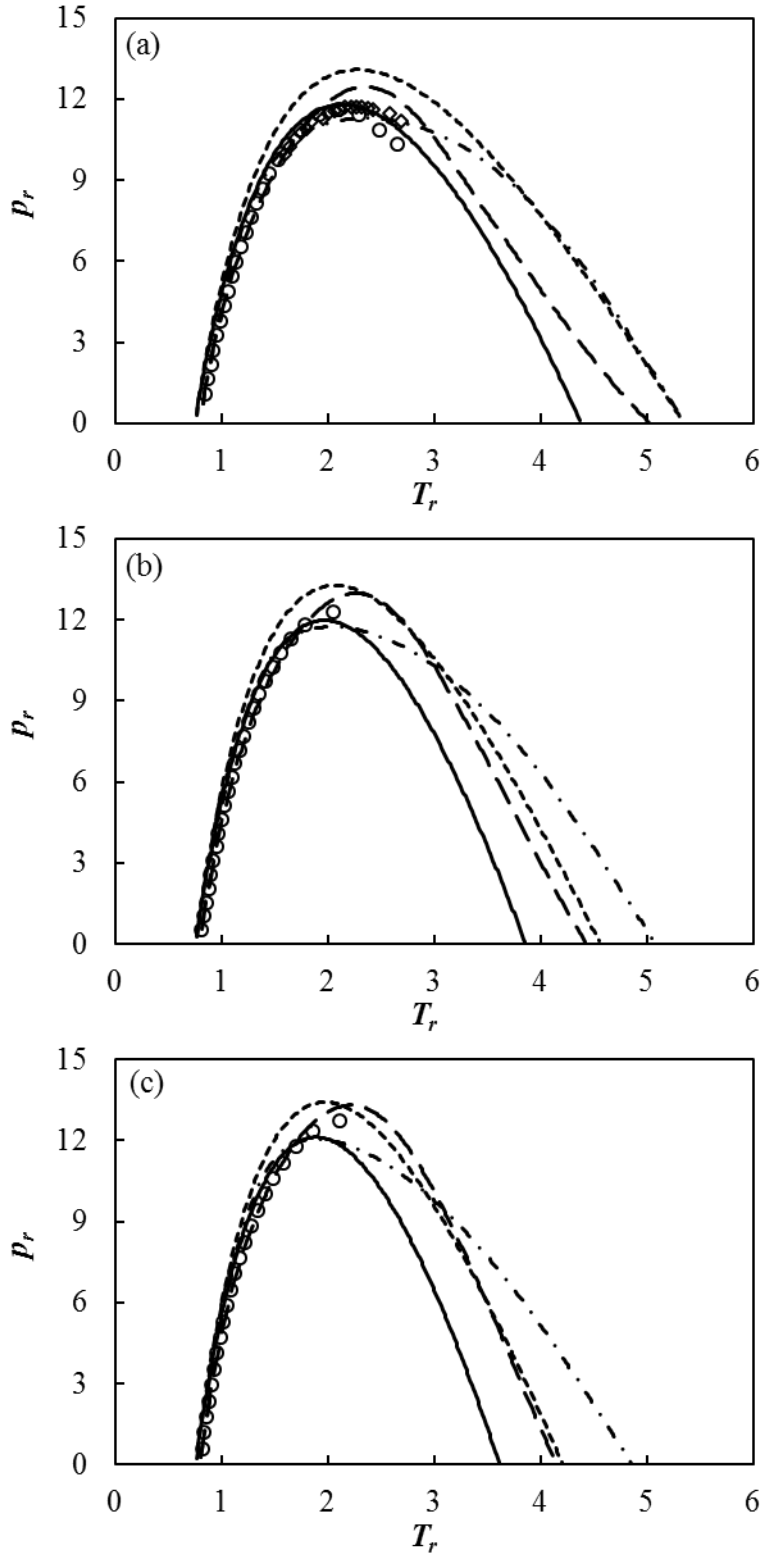

Figure 13. Calculated inversion curve for Joule-Thomson coefficient of (a) methane, (b) ethane and (c) propane through SRK (solid line), PR (dashed line), PC-SAFT (dash-dot line) and Soave-BWR (long dashed

line). Experimental data from Perry's handbook [65] (○) and Bessières et al. [21] (◇). p_r is the reduced pressure and T_r the reduced temperature.

The calculation results of the Joule-Thomson inversion curve for the six n-alkanes studied in this work are presented in Figure 14. As for the light n-alkanes, the model predictions have a good agreement in the low-temperature branch but the *pT* regions with positive Joule-Thomson coefficients predicted by the cubic EoSs are smaller than those predicted by the non-cubic models.

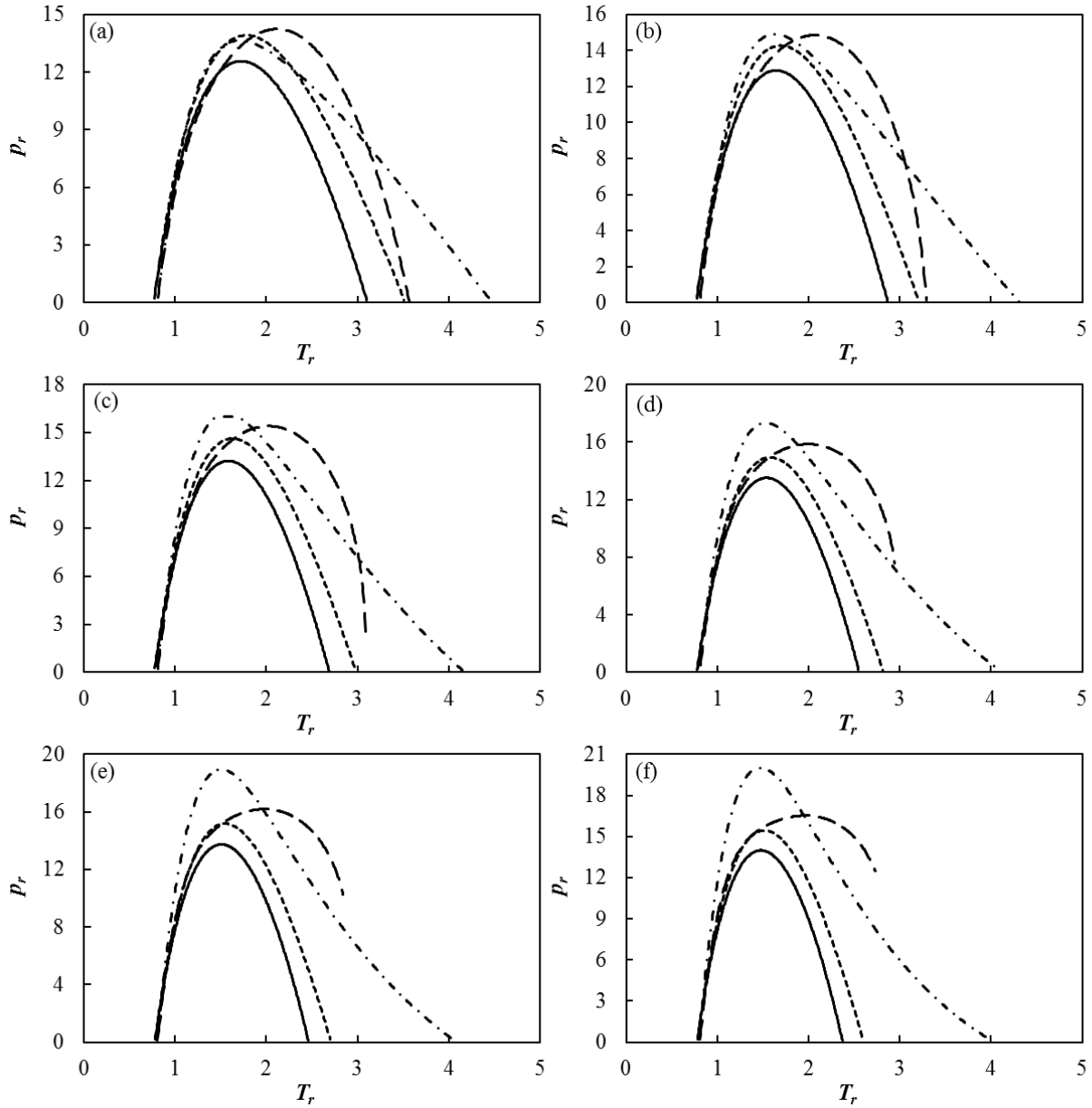

Figure 14. Predicted inversion curves for (a) n-hexane, (b) n-octane, (c) n-decane, (d) n-dodecane, (e) n-tetradecane, and (f) n-hexadecane, using different EoSs: SRK (solid line), PR (dashed line), PC-SAFT (dash-dot line) and Soave-BWR (long dashed line). p_r is the reduced pressure and T_r the reduced temperature.

Finally, in order to see how the Joule-Thomson inversion curves change with carbon number, the model predictions using PC-SAFT for the studied n-alkanes are presented in Figure 15. The calculation suggests that the peak of the inversion curve increases with the carbon number, while the maximum temperature decreases. This behaviour is also noticed for the cubic EoSs.

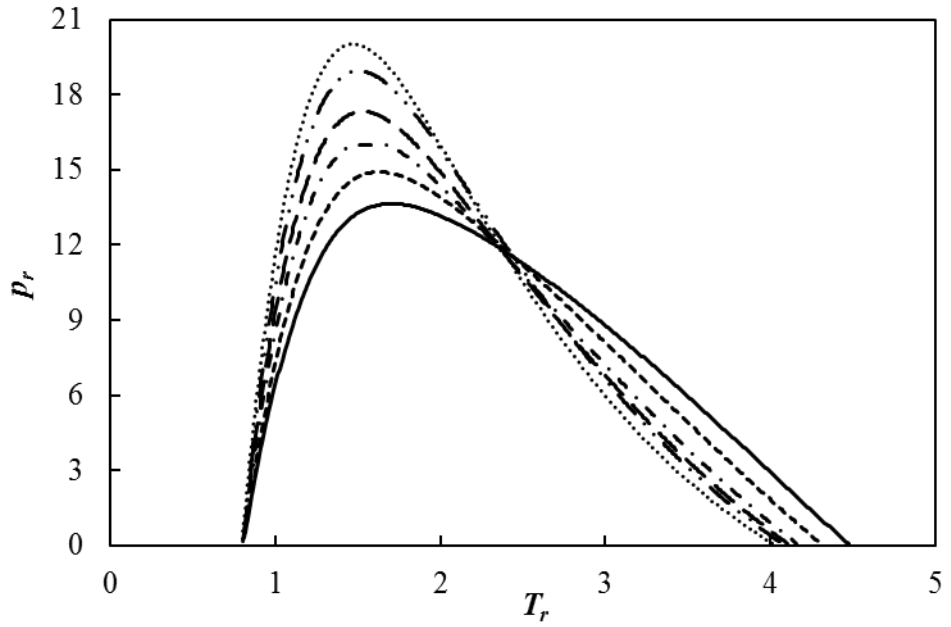

Figure 15. Predicted inversion curves for the n-alkanes studied in this work, obtained from the PC-SAFT EoS. n-hexane (solid line), n-octane (dashed line), n-decane (dash-dot line), n-dodecane (long dashed line), n-tetradecane (long dashed double dots line) and n-hexadecane (dotted line). p_r is the reduced pressure and T_r the reduced temperature.

Conclusions

Values of C_p of n-hexane, n-octane, n-decane, n-dodecane, n-tetradecane and n-hexadecane at 0.1 and 10 MPa have been measured, showing a good agreement with existing literature values with absolute average deviations of 0.38 %, 0.69 %, 0.59 %, 0.80%, 0.34 % and 0.79 %, respectively. Under the studied conditions C_p increases up to 24% with temperature, whereas the maximum change of this property with pressure from 0.1 to 10 MPa is 1.7%. As concerns the trend of specific C_p with alkyl change length, it was found that it decreases with carbon number up to n-decane or n-dodecane, whereas it remains almost constant for higher carbon numbers. Furthermore, the experimental data on C_p have been successfully predicted through four different EoSs, i.e. SRK, PR, PC-SAFT and Soave-BWR. The lower AAD was obtained for PC-SAFT (0.27%) and the highest for PR (3.05%).

The Joule-Thomson coefficients of these n-alkanes, determined from the experimental C_p data along with literature density data, are all negative under the studied experimental conditions. μ_{JT} increases with temperature, whereas it decreases with pressure and also with alkyl chain length from n-hexane to n-tetradecane, remaining almost constant for higher carbon numbers. Comparison of this property with the EoS values provided by NIST for n-hexane, n-octane, n-decane and n-dodecane gives an overall AAD of 0.7%. Regarding the prediction of the Joule-Thomson coefficient through the aforementioned models a poorer performance was obtained with the cubic EoSs, thus the worst prediction was obtained for SRK with around

46% deviation, whereas the best prediction was obtained for Soave-BWR with around 3% deviation, closely followed by PC-SAFT. As regards the prediction of the Joule-Thomson inversion curve, it was found a reasonable agreement among the four models in the low-temperature branch and also that cubic EoSs yield a smaller *pT* region of positive Joule-Thomson coefficient.

Acknowledgements

This work has been carried out in the framework of the NextOil project sponsored by Innovation Fund Denmark, DONG E&P and Maersk Oil.

References

[1] D. González-Salgado, J.L. Valencia, J. Troncoso, E. Carballo, J. Peleteiro, L. Romaní, D. Bessières, Rev. Sci. Instrum. 78 (2007) 055103.
[2] R. Páramo, M. Zouine, C. Casanova, J. Chem. Eng. Data 47 (2002) 441-448.
[3] A. Henni, Heat capacity of non-electrolyte solutions. in: E. Wilhelm, T.M. Letcher, (Eds.), Heat capacities: liquids, solutions and vapours, Royal Society of Chemistry, Cambridge, 2010, pp. 86-111.
[4] D. Bessières, H. Saint-Guirons, J.L. Daridon, High Press Res. 18 (2000) 279-284.
[5] E. Wilhelm, R. Battino, Partial molar heat capacity changes of gases dissolved in liquids. in: E. Wilhelm, T.M. Letcher, (Eds.), Heat capacities: liquids, solutions and vapours, Royal Society of Chemistry, Cambridge, 2010, pp. 457-471.
[6] V. Růžička, M. Zábranský, V. Majer, J. Phys. Chem. Ref. Data 20 (1991) 405-444.
[7] M. Zábranský, V. Růžička Jr., V. Majer, E.S. Domalski, Heat capacity of liquids. Critical review and recommended values, Monograph No. 6, Vols. I and II, Amerian Chemical Society, Washington DC, 1996.
[8] M. Zábranský, V. Růžička, E.S. Domalski, J. Phys. Chem. Ref. Data 30 (2001) 1199-1689.
[9] M. Zábranský, Z. Kolská, V. Růžička, E.S. Domalski, J. Phys. Chem. Ref. Data 39 (2010) 013103.
[10] B.A. Grigor'ev, Y.L. Rastorguev, G.S. Yanin, Izv. Vyssh. Ucheb. Zaved. Neft Gaz. 18 (1975) 63-66.
[11] M.A. Kuznetsov, V.E. Kharin, A.A. Gerasimov, B.A. Grigor'ev, Izv. Vyssh. Ucheb. Zabed., Neft i Gaz 31 (1988) 49-52.
[12] Y.M. Naziev, M.R. Mustafaev, A.A. Abasov, Proceedings of the Seventh Symposium on Thermophysical Properties (unpublished) (1977) 525.
[13] B.A. Grigor'ev, R.A. Andolenko, Izv. Vyssh. Ucheb. Zaved., Neft i Gaz 27 (1984) 60-62.
[14] J.C. Petit, L.T. Minassian, J. Chem. Thermodyn. 6 (1974) 1139-1152.
[15] D. Bessières, H. Saint-Guirons, J.L. Daridon, J.Y. Coxam, Meas. Sci. Technol. 11 (2000) N69–N72.
[16] T.S. Banipal, S.K. Garg, J.C. Ahluwalia, J. Chem. Thermodyn. 23 (1991) 923-931.
[17] D. Bessières, H. Saint-Guirons, J.L. Daridon, P. Xans, J.-Y. Coxam, J. Therm. Anal. Calorim. 51 (1998) 923-931.
[18] T.S. Khasanshin, A.P. Shchamialiou, O.G. Poddubskij, Int. J. Thermophys. 24 (2003) 1277-1289.
[19] T.S. Khasanshin, A.P. Shchemelev, High Temp. 40 (2002) 207-211.
[20] D.V. Nichita, J. Pauly, J.-L. Daridon, Int. J. Thermophys. 30 (2009) 1130-1143.
[21] D. Bessières, S.L. Randzio, M.M. Piñeiro, T. Lafitte, J.L. Daridon, J. Phys. Chem. B. 110 (2006) 5659-5664.
[22] A.C. Baker, M. Price, Modelling the performance of high-pressure high-temperature wells, European Petroleum Conference, Society of Petroleum Engineers, SPE-20903-MS, The Hague, Netherlands, 1990.
[23] C.M. Colina, M. Lísal, F.R. Siperstein, K.E. Gubbins, Fluid Phase Equilib. 202 (2002) 253-262.
[24] M. Lagache, P. Ungerer, A. Boutin, A.H. Fuchs, Phys. Chem. Chem. Phys. 3 (2001) 4333-4339.
[25] M.C. Pinto, C. Karale, P. Das, SPE Journal 18 (2013) 960-968.
[26] J.F. App, Field cases: Nonisothermal behavior due to Joule-Thomson and transient fluid expansion/compression effects, SPE Annual Technical Conference and Exhibition Society of Petroleum Engineers, SPE-124338-MS, New Orleans, Louisiana, 2009.
[27] G. Soave, Chem. Eng. Sci. 27 (1972) 1197-1203.
[28] D.-Y. Peng, D.B. Robinson, Ind. Eng. Chem. Fundam. 15 (1976) 59-64.

[29] J. Gross, G. Sadowski, Ind. Eng. Chem. Res. 40 (2001) 1244-1260.
[30] G.S. Soave, Fluid Phase Equilib. 164 (1999) 157-172.
[31] R. Abbas, C. Ihmels, S. Enders, J. Gmehling, Fluid Phase Equilib. 306 (2011) 181-189.
[32] A. Chacín, J.M. Vázquez, E.A. Müller, Fluid Phase Equilib. 165 (1999) 147-155.
[33] N.S. Matin, B. Haghighi, Fluid Phase Equilib. 175 (2000) 273-284.
[34] J. Vrabec, A. Kumar, H. Hasse, Fluid Phase Equilib. 258 (2007) 34-40.
[35] C.M. Colina, L.F. Turrens, K.E. Gubbins, C. Olivera-Fuentes, L.F. Vega, Ind. Eng. Chem. Res. 41 (2002) 1069-1075.
[36] W.G. Kortekaas, C.J. Peters, J. de Swaan Arons, Fluid Phase Equilib. 139 (1997) 205-218.
[37] F.A. Escobedo, Z. Chen, Mol. Simul. 26 (2001) 395-416.
[38] C.M. Colina, E.A. Müller, Int. J. Thermophys. 20 (1999) 229-235.
[39] J. Vrabec, G.K. Kedia, H. Hasse, Cryogenics 45 (2005) 253-258.
[40] M.H. Lagache, P. Ungerer, A. Boutin, Fluid Phase Equilib. 220 (2004) 211-223.
[41] D. Bessières, H. Saint-Guirons, J.-L. Daridon, J. Therm. Anal. Calorim. 62 (2000) 621-632.
[42] W. Wagner, A. Pruß, J. Phys. Chem. Ref. Data 31 (2002) 387-535.
[43] R. Span, W. Wagner, Int. J. Thermophys. 24 (2003) 41-109.
[44] E.W. Lemmon, R. Span, J. Chem. Eng. Data 51 (2006) 785-850.
[45] E.W. Lemmon, M.L. Huber, Energy Fuels 18 (2004) 960-967.
[46] T. Regueira, W. Yan, E.H. Stenby, J. Chem. Eng. Data 60 (2015) 3631-3645.
[47] J. Gross, G. Sadowski, Ind. Eng. Chem. Res. 41 (2002) 1084-1093.
[48] N. von Solms, I.A. Kouskoumvekaki, M.L. Michelsen, G.M. Kontogeorgis, Fluid Phase Equilib. 241 (2006) 344-353.
[49] M. Benedict, G.B. Webb, L.C. Rubin, J. Chem. Phys. 8 (1940) 334-345.
[50] W. Yan, F. Varzandeh, E.H. Stenby, Fluid Phase Equilib. 386 (2015) 96-124.
[51] T.E. Daubert, R.P. Danner, Physical and Thermodynamic Properties of Pure Compounds: Data Compilation, Hemisphere, New York, 2001.
[52] J.M. Mollerup, M.L. Michelsen, Fluid Phase Equilib. 74 (1992) 1-15.
[53] G. Widmann, R. Riesen, Thermal analysis, Hüthig-Verlag, 1987.
[54] E. Gmelin, S.M. Sarge, Pure Appl. Chem. 67 (1995) 1789-1800.
[55] C.A. Cerdeiriña, C.A. Tovar, D. González-Salgado, E. Carballo, L. Romaní, Phys. Chem. Chem. Phys. 3 (2001) 5230-5236.
[56] Z.I. Zaripov, S.A. Burtsev, A.V. Gavrilov, G.K. Mukhamedzyanov, Theor. Found. Chem. Eng. 36 (2002) 400-405.
[57] R. Burgdorf, A. Zocholl, W. Arlt, H. Knapp, Fluid Phase Equilib. 164 (1999) 225-255.
[58] C.A. Cerdeiriña, C.A. Tovar, E. Carballo, L. Romaní, M. del Carmen Delgado, L.A. Torres, M. Costas, J. Phys. Chem. B. 106 (2002) 185-191.
[59] J.A. Gates, R.H. Wood, J.C. Cobos, C. Casanova, A.H. Roux, G. Roux-Desgranges, J.-P.E. Grolier, Fluid Phase Equilib. 27 (1986) 137-151.
[60] W.G. Schlinger, B.H. Sage, Ind. Eng. Chem. 44 (1952) 2454-2456.
[61] G. Salvetti, C. Ferrari, E. Tombari, Thermochim. Acta 316 (1998) 47-56.
[62] Y. Coulier, K. Ballerat-Busserolles, J. Mesones, A. Lowe, J.-Y. Coxam, J. Chem. Eng. Data 60 (2015) 1563-1571.
[63] D. Huang, S.L. Simon, G.B. McKenna, J. Chem. Phys. 122 (2005) 084907.
[64] E.W. Lemmon, M.L. Huber, M.O. McLinden, NIST Reference Fluid Thermodynamic and Transport Properties Database (REFPROP): Version 9.1, 2013.
[65] R.H. Perry, D.W. Green, Perry's Chemical Engineers' Handbook, 7th ed., McGraw-Hill, 1998.